Taylor & Francis
Taylor & Francis Group

Spectroscopy Letters

An International Journal for Rapid Communication

ISSN: 0038-7010 (Print) 1532-2289 (Online) Journal homepage: http://www.tandfonline.com/loi/lstl20

Structure correlation of silylated dicarboxylic acid monomer and its respective oligomeric polyamide-imide using experimental and theoretical vibrational spectra

Carmen M. González-Henríquez, Claudio A. Terraza, Mauricio A. Sarabia, Alejandra M. Vera & Álvaro E. Aliaga

To cite this article: Carmen M. González-Henríquez, Claudio A. Terraza, Mauricio A. Sarabia, Alejandra M. Vera & Álvaro E. Aliaga (2017) Structure correlation of silylated dicarboxylic acid monomer and its respective oligomeric polyamide-imide using experimental and theoretical vibrational spectra, Spectroscopy Letters, 50:1, 30-38, DOI: 10.1080/00387010.2017.1282523

To link to this article: http://dx.doi.org/10.1080/00387010.2017.1282523

Accepted author version posted online: 19 Jan 2017.
Published online: 19 Jan 2017.

SPECTROSCOPY LETTERS
2017, VOL. 50, NO. 1, 30–38
http://dx.doi.org/10.1080/00387010.2017.1282523

Taylor & Francis
Taylor & Francis Group

Structure correlation of silylated dicarboxylic acid monomer and its respective oligomeric polyamide-imide using experimental and theoretical vibrational spectra

Carmen M. González-Henríquez[a], Claudio A. Terraza[b], Mauricio A. Sarabia[c], Alejandra M. Vera[d], and Álvaro E. Aliaga[d]

[a]Departamento de Química, Facultad de Ciencias Naturales, Matemáticas y del Medio Ambiente, Universidad Tecnológica Metropolitana, Santiago, Chile; [b]Facultad de Química, Pontificia Universidad Católica de Chile, Santiago, Chile; [c]Departamento de Ingeniería Estructural y Geotecnia, Pontificia Universidad Católica de Chile, Santiago, Chile; [d]Departamento de Química, Universidad de Chile, Facultad de Ciencias, Santiago, Chile

ABSTRACT

Correlation between theoretical and experimental (infrared and Raman spectroscopies) vibrational spectra of two compounds, both with a silyl group present in their main chain and with an optically active structure (L-valine) as side group, was performed. These compounds are based in a chiral dicarboxylic acid monomer and its respective polyamide-imide, oligomer that was previously synthesized by a direct polycondensation. Spectra were recorded in the region comprised between 500 and 4000 cm^{-1} for infrared and Raman analysis. The Raman spectra were obtained through a 1064 nm laser as excitation source.

Theoretical models were carried out in order to find the optimal molecular geometry of the analyzed systems, with a complete assignment of their vibrational spectra. The Raman experimental data obtained with a Nd:YAG laser for this kind of silylated organic compounds, and the comparison between these results with the theoretical data is a useful advance in the polymer synthesis field, which can be used as reference for subsequent studies.

ARTICLE HISTORY
Received 3 October 2016
Accepted 11 January 2017

KEYWORDS
Infrared and Raman spectroscopy; modeling and simulation; organo-metallic compounds; polymer composites

Introduction

Infrared and Raman spectroscopies are complementary techniques used in molecular structure determination, compounds identification, and for the study of possible interactions or changes of the molecular symmetry,[1] among others. Specially, some Raman applications have been used in diverse fields such as: nanoparticles identification,[2] pigment in artistic paints,[3] archeological artifacts,[4] forensic science,[5] cancer diagnosis, analysis of cells and extracellular matrix components in tissues in the biomedical field,[6] among others.

An important advantage of both the techniques is the low amount of compound required for analysis. However, some limitations of infrared and Raman spectroscopies are related with the detection of monoatomic ions, homonuclear diatomic molecules, the analysis of complex mixtures, the overlapping and subsequent masking of certain weak bands due to fluorescence processes. In order to solve this last problem, different theoretical methods such as mathematical polynomial approaches,[7] experimental techniques as different types of laser (Nd:YAG) for interaction with the sample,[8] quenching process (graphene deposition),[9] and certain chemical compounds or nanoparticles[10] have been used recently. Today, Raman data also could be associated to the theoretical calculations using density functional theory (DFT) methods by spectrum simulation, becoming in an interesting way to understand the behavior of some systems that show difficulties in their study and in interpretation of results or analysis.[11,12]

Studies related to vibrational analysis associated with experimental and theoretical methodologies are based on terpene chemistry[13] and the effect of secondary structures in terms of localized vibration modes such as amide I-II bands.[14] The finality of these researches are related to structural determination, stereochemistry configuration that plays important roles in different fields, such as pharmacology efficacy (chiral drug)[15] and environment contamination (chiral pesticide),[16] among others.

Generally, the organic polymers manifest high fluorescence leading to problems at the moment of identifying weak Raman vibrations. Herein, experimental (Infrared and Raman spectroscopies) and theoretical studies of chiral dicarboxylic acid monomer (**L-VAL**) and its respective oligomeric polyamide-imide (**PALV**) were performed and analyzed in detail. **PALV** was synthesized previously by our research group, using a typical polycondensation between **L-VAL** and an aromatic diamine (bis(4-aminophenyl)diphenylsilane) (**DIA**).[17] A laser beam of 1064 nm (infrared) was used as excitation light for record Raman spectra. The long infrared wavelength prevents the energy absorption, eliminating or reducing the fluorescence of the compounds in most of the cases.[18]

On the other hand, DFT calculations based on Becke's three parameter hybrid model using the Lee-Yang-Parr correlation functional (B3LYP) method were applied. This kind of procedure has proven to be an excellent tool for the association of a vibrational pattern with a particular frequency, process that facilitates the detection and identification of certain

CONTACT Carmen M. González-Henríquez carmenmabel@gmail.com Departamento de Química, Facultad de Ciencias Naturales, Matemáticas y del Medio Ambiente, Universidad Tecnológica Metropolitana, P.O. Box 9845, Correo 21, 7800003, Santiago, Chile.
Color versions of one or more of the figures in the article can be found online at www.tandfonline.com/lstl.

functional groups in organic and inorganic polymers from different classes and nature.[19,20] The calculated vibrational wavenumbers were compared with the experimental (Infrared and Raman spectra) results obtained.

Experimental procedure

Materials and methods

As mentioned previously, chiral dicarboxylic acid monomer, (2R,2′S)-2,2′-(5,5′-(diphenylsilanediyl)bis(1,3-dioxoisoindoline-5,2-diyl))bis(3-methylbutanoic acid) (**L-VAL**), was prepared according to a procedure described in the literature.[17] On the other hand, oligomeric polyamide-imide (**PALV**) was synthetized from an aromatic diamine (bis(4-aminophenyl) diphenylsilane (**DIA**)[17,21,22] and **L-VAL** (1:1 mol/mol) by using the Yamazaki's direct polycondensation methodology.[23–25] A complete experimental characterization for **DIA** monomer was already published by our research group.[11]

Optical rotations of the systems were measured at concentrations of 5 and 10 mg dL^{-1} in dimethylformamide (DMF) at 17°C using as reference the wavelength of the D-line of sodium ($\lambda = 589.3$ nm) through a CIENTEC automatic polarimeter manufactured by Optical Activity Ltd.[17] Results show that both monomeric and oligomeric mixtures are optically active (levorotatory enantiomers), with specific optical rotation of $-53.7°dm^{-1}g^{-1}cm^3$ and $-17.2°dm^{-1}g^{-1}cm^3$, respectively.

Samples for infrared were prepared using KBr disc technique commonly used for solid (powder) samples. Spectra of the molecules were recorded in the 500–4000 cm^{-1} region using a Perkin-Elmer FT-IR 1310 spectrometer. Raman analysis was performed with a portable Raman (BWTEC BWS485) equipped with a Nd:YAG laser beam (1064 nm), InGaAs array detector with deep thermoelectric cooling using a spectral coverage range from 500 cm^{-1} to 4000 cm^{-1} with 20 accumulations for sample.

Computational details

All the calculations were performed using Gaussian03 software, Revision D.02 program package for personal computer, being chosen to perform geometry optimization frequency calculations, whose results were associated to a certain vibration.[26] All the calculation was performed on isolates systems using the Becke's three parameter B3LYP exchange correlation functional, together with Pople's 6-31G* basis set.[27] Due to the combination of electron correlation effect and basis set deficiencies, the calculated harmonic frequencies are found higher than the experimentally observed frequencies. So, the results were scaled down uniformly by a factor of 0.9613 as recommended by Wong,[28] which minimized the error between the experimental and the calculated harmonic frequencies, correcting for the approximate treatment of electron correlation, for basis set deficiencies and for anharmonicity. The advent of density functional theory (DFT) has provided an alternative means of including electron correlation in the study of the vibrational frequency of moderate large molecules.[29,30]

On the other hand, all the vibrational assignments are based on the respective point group of symmetry for the molecule; the visualization of the atomic displacement representation for each vibration was performed through GAUSSVIEW 09W and posteriorly matched with the predicted normal wavenumber and intensities using the experimental data.

Results and discussion

Infrared and Raman spectroscopy

Molecular structure of **L-VAL** and **PALV** exhibits chirality. Optical isomers of the same compound as mirror images have identical vibrational spectra and therefore same vibrational modes, since they have the same structure and symmetry.

Experimental wavenumbers observed in the infrared and Raman spectra and their respective theoretical assignments are shown in Tables 1 and 2. These values correspond to vibration treated with the scaling factor (0.9613).[28] Thus, theoretical and experimental (Infrared and Raman) bands were summarized in these tables so as to enable an ordered visualization of the data.

Table 1. Comparison of experimental and theoretical central peak wavenumbers for chiral dicarboxylic acid monomer obtained by Raman and infrared spectroscopies.

	Experimental		
Vibration	Raman	Infrared	Theoretical
OH stretch, H-bonded	-	3427 (broad)	3446 (m)
Aromatic CH stretch	-	3071, 3051 (w)	3074 (m)
CH_3 (antisymmetric) and CH stretch	-	2967 (mw), 2929 (w)	2984, 2935 (w)
C=O cyclic imides (*ip* and *oop*) and C=O stretch, monomer and dimer H-bonded of carboxylic acid	1774 (s), 1725 (w)	1776 (m), 1726 (s)	1774 (m), 1726 (s)
C=C stretch (in ring)	1613, 1590 (m)	1642, 1611, 1590 (w)	1618 (m)
Aromatic C-Si and C=C ring stretch	1572 (w)	1547 (w)	–
COH *ip* bend of carboxylic acid	1466 (w)	1467 (w)	1475 (w)
CH_3 antisymmetric/symmetric bend deformation	1417 (mw), 1377 (mw), 1330 (w)	1414 (m), 1376 (ms)	1398, 1371 (w)
CNH stretching	1266 (vw)	1266 (mw)	1269 (mw)
CO stretch of carboxylic acid	1195 (m)	1209, 1188 (mw)	1208, 1189 (w)
CH *ip* bending and ring torsion, mono subst. R-C_6H_5	1111 (w), 1064 (w), 1003 (s)	1109, 1079 (m), 1060 (w)	1131, 1068, 1005 (m)
OH *oop* bend	926 (w)	920 (m)	948 (mw)
CH *oop* bend and ring torsion, tri subst. R_3-C_6H_3. Aromatic C-Si bend	849 (mw), 711 (m)	843 (w), 745 (m)	849 (w), 753 (m)
CH bending (*oop*), mono subst. R-C_6H_5	696, 658, 623 (w)	698 (m), 651 (mw)	701, 688 (w)

oop = Out-of-plane. *ip* = In-plane.

Table 2. Comparison of experimental and theoretical central peak wavenumbers for oligomeric polyamide-imide obtained by Raman and infrared spectroscopies.

	Experimental		
Vibration	Raman	Infrared	Theoretical
NH and OH stretch	–	3433 (broad), one band for 2° amide	3457 (m)
Aromatic CH stretch	–	3070 – 3050 (w), three bands	3092 (s)
CH_3 (antisymmetric) and CH stretching.	–	2966 (mw)	2986 (w)
C=O cyclic imides (*ip* and *oop*) and C=O amide stretch **Amide I.**	1784 (m), 1687 (mw)	1774 (m), 1716 (s)	1776 (m), 1695 (s)
C=C ring stretch	1625 (m), 1594 (s)	1592 (m)	1591 (s)
Si-C aromatic, C=C ring stretch and **amide II.**	1523 (m)	1511 (m)	-
CNH stretch-bend	1431 (vw)	1493 (m)	1491 (w)
CH_3 antisymmetric /Symmetric bend deformation.	1385 (w)	1429 (w), 1412 (w)	1418 (w), 1388 (mw)
OH *ip* bend, C-H and NH bend	1325 (m)	1373, 1355 (m)	1386 (m), 1332 (mw)
Extended amide **III mode.**	1296, 1246 (m)	1247 (mw)	1295 (m)
CO stretch.	1197 (m)	1190 (mw)	1193 (m)
CH *oop* and *ip* bend, ring torsion, -R-C_6H_5	1106 (s), 1035 (w), 1000 (s)	1113 (m), 1076 (m), 1028 (w), 996 (w)	1127, 1086, 1011 (mw)
CH *oop* bend and ring torsion, tri subst. R_3-C_6H_3 aromatic C-Si bend	943 (w), 873 (w)	921 (mw), 825 (w)	929, 884 (w)
CH *oop* bend, mono subst. R-C_6H_5 and NH (*oop*).	771 (w)	741 (mw), 700 (m)	742, 710 (w)
Ring deformation mode (mono and tri. subst.)	672 (mw)	601 (w)	653 (w)

oop = Out-of-plane, *ip* = In-plane.

Chiral dicarboxylic acid monomer (L-VAL)

Figure 1 (left) shows the molecular structure of **L-VAL**; this compound contains a silicon atom within its structure that promotes its flexibility and also increases its ionic nature. Moreover, the structural conformation is seriously affected by the torsion angles of the phenyl groups around the tetravalent metalloid as is possible to observe in the tridimensional optimization (Fig. 1, right). This characteristic produces a Raman spectrum with high fluorescence. These characteristics affect signal positioning and intensities of some vibrational bands that are observed by infrared and Raman spectroscopies. All vibrational spectra assignments were based on the respective symmetry group of each system; $\hat{C}_2$ for **L-VAL** and $\hat{C}_1$ for **PALV**.[11,31]

Figure 2 shows the theoretical and experimental spectra of **L-VAL** (Raman and infrared) carried out in solid state (powder). The spectra are mainly dominated by the contribution of the rigid part of the molecule (CH and C=C aromatic group), aliphatic moieties (CH_3, CH_2, CH), OH, C=O (carboxylic acid

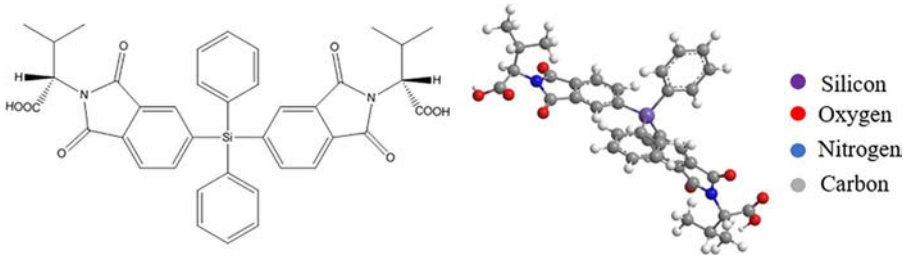

Figure 1. Molecular structure of chiral dicarboxylic acid monomer and their tridimensional optimization.

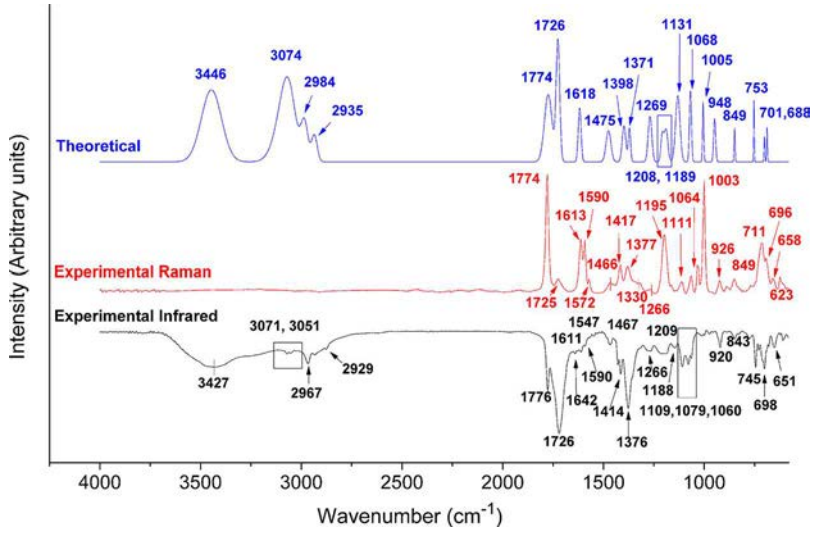

Figure 2. Spectra of chiral dicarboxylic acid monomer for Theoretical (blue line), Experimental Raman (red line), and Experimental Infrared (black line).

and cyclic imides) among other vibrational modes. The assignation of bands for the monomer is detailed and summarized in Table 1.

Bands from 3500 to 1700 cm^{-1}

The OH carboxylic acid stretching shows very weak scattering in the Raman spectra, so, IR data are generally used for identifying this vibration. Thus, at 3427 cm^{-1}, a complex band (broad) is assigned to hydrogen-bonded OH stretch, which is associated to combination with intermolecular dimeric and intramolecular bridge. The same vibration is predicted by theoretical simulations at 3446 cm^{-1} with a medium intensity.

The OH stretch is superposed to the bands related to CH stretching vibration in aromatic groups due to its breadth. Thus, the aromatic CH stretching of substituted benzenes usually generates IR and Raman bands in the region comprised between 3100–3000 cm^{-1}. Experimentally, by infrared the monomer shows a doublet at 3071 and 3051 cm^{-1} with weak intensities, which is predicted through DFT theory as one signal located at 3074 cm^{-1} with medium intensity. The last mentioned vibration was not obtained experimentally by Raman spectroscopy.

Although the aliphatic CH stretching bands appear below 3000 cm^{-1}, the CH_3 antisymmetric and symmetric stretching vibrational modes are found near to 2967 cm^{-1} (medium-weak) and 2929 cm^{-1}(weak), respectively. These results (intensity and displacement) are attributable to the low symmetry of the monomer. In the present case, theoretical calculation shows two vibration modes at 2984 cm^{-1} and 2935 cm^{-1}, both showing weak intensities. It is very important to mention that these vibrations are not pure due to the contention of significant contributions of other modes. For example, CH stretching is often obscured by the much stronger CH_3 stretching band in both IR and Raman spectra.

In the region comprised between the wavelengths 2623 and 2322 cm^{-1}, the overtones and band combination of radical groups are located near to 1467 cm^{-1} and 1209–1188 cm^{-1} that correspond to COH (*ip*) bending and CO stretching, respectively (infrared spectroscopy).

Carboxylic acids, presented as dimer, show a strong antisymmetric band that could be overlapped with the cyclic imide five membered rings (generally with two characteristic bands). The in-phase and out-phase appear at 1776 cm^{-1} (medium) and 1726 cm^{-1} (strong), respectively, and these results were obtained by experimental infrared; this last band is associated also to the C=O antisymmetric vibration. Experimental Raman shows the same vibrations to 1774 cm^{-1} (strong, active) and 1725 cm^{-1} (weak, inactive).[32] Theoretical simulation predicts the apparition of these modes at 1774 cm^{-1} (medium) and 1726 cm^{-1}(strong), respectively.

Bands from 1700 to 1200 cm^{-1}

Experimental infrared spectrum shows in the region comprised between the wavelengths 1642 and 1590 cm^{-1} three weak bands that could be associated to *ip* CH bending that interacts with various C=C ring vibrations. These normal modes appear in the 1450–1650 cm^{-1} region for the benzene derivate.[33] In this case, bands located at 1613, 1590 cm^{-1} for Raman spectra were visualized with medium intensity. Additionally, these vibrations were predicted using DFT methods at 1618 cm^{-1}(medium).

Experimental Raman spectrum (Fig. 2) showed two weakly peaks at 1572 cm^{-1} and 849 cm^{-1} attributed to a Si-phenyl vibration (antisymmetric stretching and bending, Fig. 3). Same absorption bands were obtained at 1547 cm^{-1}(symmetric stretching) and 843 cm^{-1} through experimental infrared.[34] This vibration band is clearly overlapped with characteristic modes of the benzene ring.

A band is reported at 1467 cm^{-1} and 1466 cm^{-1} with weak intensities by experimental infrared and Raman spectra, respectively (Fig. 2). These bands are related to COH *ip* bending vibration of the carboxylic acid dimer bands. A weak signal is theoretically obtained at 1475 cm^{-1} (DFT).

In the experimental data obtained with infrared technique, the antisymmetric and symmetric CH_3 bendings were observed at 1414 cm^{-1}(medium intensity) and at 1376 cm^{-1} (medium-strong intensity), respectively. Experimental Raman spectrum shows three bands at 1417 cm^{-1} (medium-weak), 1377 cm^{-1} (medium-weak), and 1330 cm^{-1} (weak) with opposite relative peak intensity than that obtained through experimental infrared. DFT method predicts bands for this vibration at 1398 cm^{-1} and 1371 cm^{-1} with weak intensities. The tertiary CH bending occurs near to 1355 cm^{-1} (shoulder of a strong band at 1376 cm^{-1} that corresponds to a CH_3 deformation) with weak intensity in the infrared spectrum and near to 1330 cm^{-1} for experimental Raman spectrum. However, the use of this vibrational mode as a group reference is limited unless there is no spectral reference in this region.[35]

At 1266 cm^{-1}, a medium-weak band is observed in the infrared spectra, which is related to the CNH stretch. Same vibrations located at 1269 cm^{-1}(medium-weak) were predicted by DFT. This band type is also observed with very weak intensity at 1266 cm^{-1} in the experimental Raman spectra.

Two bands located at 1209 cm^{-1} and 1188 cm^{-1} were observed in the experimental infrared spectra with medium-weak intensities, signals that are related to CO stretching of

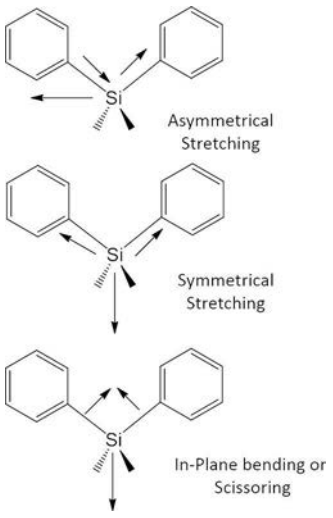

Figure 3. Some Si-C aromatic bond vibrations: Stretching at 1572 cm^{-1} (Experimental Raman), stretching at 1547 cm^{-1} (Experimental infrared), and bending at ~849 cm^{-1} (Experimental infrared and Raman).

carboxylic acid group. The corresponding band – theoretically calculated – can be located at 1208 cm^{-1} and 1189 cm^{-1} with weak intensities. This same vibrational normal mode was observed in the experimental Raman spectra at 1195 cm^{-1} with a signal moderately strong (medium).

Bands from 1200 to 600 cm^{-1}

In aromatic compounds, the CH *ip* bending wavenumber appears in the range comprised between 1000–1200 cm^{-1} and the CH *oop* bending vibrations in the region limited by 700–1000 cm^{-1}; the aromatic ring vibration mode occurs near to ~840 cm^{-1}.[36] In agreement with this, the bands that appear near to 1109 cm^{-1}(medium), 1079 cm^{-1} (medium), and 1060 cm^{-1} (weak) could be associated to the in-phase CH aromatic ring and phenyl groups. Additionally, these same vibration modes, with medium intensities, were predicted via theoretical methods at 1131, 1068, and 1005 cm^{-1}. Experimentally, the Raman spectrum shows three signals located at 1111 cm^{-1} (weak), 1064 (weak), and 1003 cm^{-1} (strong). Together with these bands, a monosubstituted benzene shows three possible vibrations corresponding to *oop* CH wagging located at 696, 658, and 623 cm^{-1} (weak, experimental Raman spectrum), which were theoretically predicted by DFT at 701 and 688 cm^{-1}. Experimental infrared presents two bands with medium and medium-weak intensities, respectively, that were established at 698 and 651 cm^{-1}.

Trisubstituted benzenes (three adjacent hydrogens) show characteristic bands related to the CH *oop* wagging, which also could be overlapped with the C-Si bending. Thus, at 849, 711 cm^{-1} (medium-weak, medium intensities) and 849, 753 cm^{-1} (weak, medium intensities) were observed by 'experimental and theoretical Raman, respectively. The results obtained include a large contribution from the *oop* vibrations of the aromatic rings, whose intensity seems increased due to the predominant flat orientation of the phenyl groups bonded to the silicon atom. These same signals are obtained in the experimental infrared at 843 cm^{-1}, 745 cm^{-1} (weak, medium intensities).

Finally, a band related to OH *oop* wagging appears at 920 cm^{-1} with medium intensity in the experimental infrared spectrum and also at 948 cm^{-1} (medium-weak) using DFT methods. Additionally, the same vibration band can be located at 926 cm^{-1} (weak) in the experimental Raman spectrum obtained.

Theoretical graphs present the significant feature bands with their respective intensities, showing clear tendency of the vibration obtained by DFT and the experimental results. Theoretical spectra were plotted using fitting software that permits the adjusting of Gaussian-Lorentzian peaks with different Full Width Half Maximum (FWHM), in order to emulate experimental spectrum, centered at values obtained by B3LYP/6-31G* model. According to this, the major theoretical intensity is associated to the C=O stretching polarizability of the compounds (cyclic imide, monomer, and H-bonded dimer), results that are consistent with the experimental studies.

Finally, the discrepancy between experimental and theoretical (calculated) vibration results is attributable to conformational isomers, corresponding to different orientation of the chiral carbon, that present the molecule. Similar case is showed in the assignment of 1,1,2-trifluro-2-methoxypropane or study on the radical, monomer, and dimer of α-keto pyruvic acid.[37,38] Examples of these values – discrepancies and loss signals – are: CH_3 antisymmetric/symmetric bend deformation and CH bending (*oop*) mono. sub. R-C_6H_5, among others vibrations.

Oligomeric polyamide-imide (PALV)

The characterization of this system was realized previously by our research group[17]; according to this, the molecular mass obtained by MALDI-TOF mass spectrometry is 3381 m/z (Repeat unit: 1100 g mol^{-1}, molecular mass: 3358 g mol^{-1}). In agreement with these results, **PALV** is an oligomer constituted of three repetitive units (n = monomeric units) of low molecular masses, as is possible to observe in their molecular structure (Fig. 4, left). Additionally, this compound presents a glass transition temperature of 144°C, an initial decomposition temperature of 5% mass loss at 298°C and of 10% mass loss at 376°C, thermal behavior that was established by DSC and TGA techniques, respectively.

PALV was synthesized through the reaction between **DIA** and **L-VAL**. Both monomers show two benzene rings, which are coplanar with the silicon atom in the central part of the structure (diphenylsilane moiety). Thus, the flexibility of the resulting system is given by symmetry breaking and, also due to the presence of aliphatic pendant groups promoted by the chiral aminoacid employed during the synthesis, characteristic that can be visualized through an optimized tridimensional scheme (Fig. 4, right).

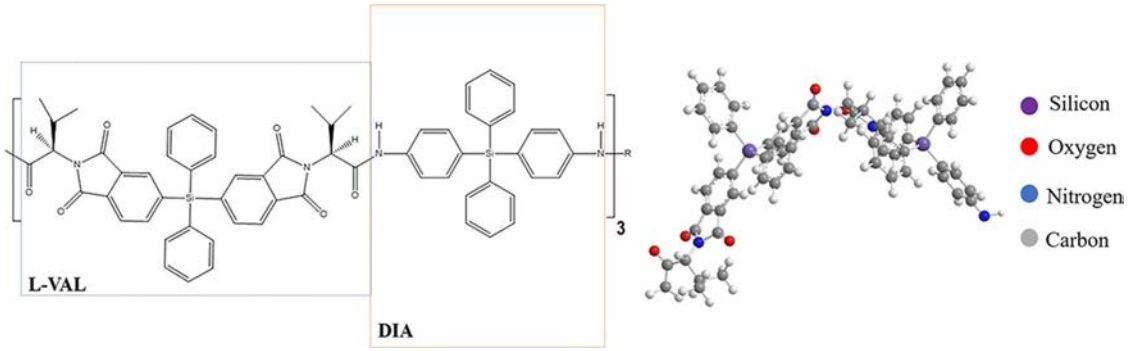

Figure 4. Molecular structure of the repetitive unit of oligomeric polyamide-imide and their tridimensional optimization.

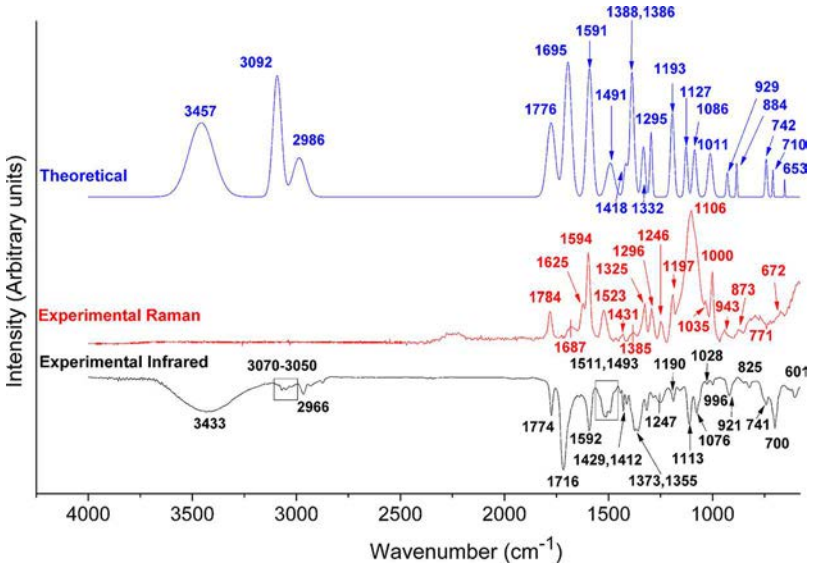

Figure 5. Spectra of oligomeric poly(amide-imide) for Theoretical (blue line), Experimental Raman (red line), and Experimental Infrared (black line).

Theoretical and experimental (Raman and infrared) spectra were obtained for **PALV** (Fig. 5). The performed band assignment is displayed in Table 2.

Reported Raman spectrum of monomer and oligomer shows slight differences between them (Figs. 2 and 5). An example is attributed to the amide I vibration, whose frequency can be found in the $1600 - 1700\ cm^{-1}$ range.[39] In the oligomer spectrum, this normal mode appears near to $1687\ cm^{-1}$ with medium-weak intensity; however, this band was not observed in the monomer spectra (Fig. 2). The amide I band is related to the C=O stretching coupled with the CN bond and is present with very strong intensity in theoretical predictions ($1695\ cm^{-1}$). Additionally, the band position is determined by the backbone conformation of the oligomer and also to the hydrogen bonding pattern established in its structure, indicating that maybe the structure presents a β turn in the bond with the amino acid residue, very common in this kind of structures.[40]

Bands from 3500 to 1700 cm^{-1}

In the experimental infrared spectrum, most of the peaks that appear in the range of 3433–2966 cm^{-1} are associated to NH, OH, CH_3, CH, and aromatic CH stretching vibrational modes. Thus, NH asymmetric stretch, which is associated to secondary amide mode, can be seen in the oligomer spectrum as a broad peak located at 3433 cm^{-1}; these vibrations modes were predicted as medium intensity bands via the application of DFT methods (3457 cm^{-1}).

The aromatic CH stretch exhibits multiple bands in the region comprised between 3070 cm^{-1} and 3050 cm^{-1} with weak intensities in the experimental infrared spectrum. Additionally, DFT calculations show vibrations of CH modes at 3092 cm^{-1} (strong intensity).

Antisymmetric CH_3 and CH stretching occurs at 2966 cm^{-1} with medium-weak vibration intensity observed only in the experimental infrared spectrum. These theoretical asymmetric bands were located near to 2986 cm^{-1} with weak intensity. It should be noted that the NH and OH, aromatic CH, antisymmetric CH_3, and CH stretching vibrational modes could not be visualized by experimental Raman spectrum.

Raman bands at 1784/1687 cm^{-1} (medium/medium-weak intensities) were obtained experimentally by Raman spectroscopy. These vibrations are associated with C=O *ip* and *oop* stretching modes (cyclic imide and amide functions); in addition, the bands calculated by DFT methods for this vibrational modes are 1776 cm^{-1} and 1695 cm^{-1} with medium and strong intensities, respectively. Experimental infrared spectrum shows two signals at 1774 cm^{-1} (medium) and at 1716 cm^{-1} (strong).

Bands from 1700 to 1200 cm^{-1}

Experimental Raman shows two bands that were assigned as C=C ring stretching located at 1625 cm^{-1} and 1594 cm^{-1} with medium and strong intensities, respectively. For experimental infrared, this signal was founded at 1592 cm^{-1} (medium intensity). The same bands were theoretically calculated at 1591 cm^{-1} with a strong intensity by DFT methods.

The Si-C aromatic stretching band was observed at 1523 cm^{-1} for experimental Raman spectra and at 1511 cm^{-1} for experimental infrared spectrum, both with medium intensities. These vibrations values were not obtained through theoretical methods; neither for the polymer or for the monomer, probably this mode could be overlapped with the benzene rings bands.

Experimental Raman scattering of CNH stretch-bending was obtained at 1431 cm^{-1} with very-weak intensity. Additionally, this band at 1491 cm^{-1} with weak intensity was predicted through DFT. This vibration mode is also observed in the experimental infrared spectra at 1493 cm^{-1} with a medium intensity (Fig. 5).

The antisymmetric and symmetric CH_3 bending appears at 1470–1430 cm^{-1} and 1395–1365 cm^{-1}, respectively.[35] In our case, these vibrations were located at 1385 cm^{-1} for experimental Raman and at 1429 and 1412 cm^{-1} for

experimental infrared. Same bands were theoretically predicted at 1418 cm^{-1} (weak) and 1388 cm^{-1} (medium-weak) by DFT, respectively.

The OH bending is coupled with the CH bending and with the NH deformation (amide III), showing medium bands centered at 1373, 1355 cm^{-1} and at 1325 cm^{-1} for experimental infrared and Raman spectra, respectively. Values and intensities were similar than the theoretically predicted: 1386 cm^{-1} (medium) and 1332 cm^{-1} (medium-weak).

On the other hand, the bands that appear at 1296 and 1246 cm^{-1} are related to the extended amide III region (Raman active groups) and to the skeletal vibration with weak intensities located at 943 and 873 cm^{-1}. The first band appears centered at 1247 cm^{-1} in the experimental infrared spectra and theoretically founded in 1295 cm^{-1} using DFT methods. These data suggest a randomly disordered spatial conformation of the chiral polymer.[41] Finally, the signal for the amide II band is not clearly visualized, probably because it is overlapped with the Si-C aromatic stretching vibration.

Bands from 1200 to 600 cm^{-1}

At 1197 cm^{-1}, a band with medium intensity was obtained in the experimental Raman; this band was assigned to a CO vibration mode. For infrared spectra at 1190 cm^{-1} is observed the same vibration with medium-weak intensity. Additionally, a band at 1193 cm^{-1} (medium intensity) was theoretically obtained using DFT method.

Bands assigned as CH *oop, ip* and ring torsion bending vibrations (-R-C_6H_5) involucre three values in the experimental Raman spectrum located at 1106 cm^{-1} (strong), 1035 cm^{-1} (weak). and 1000 cm^{-1} (strong). By DFT calculations, different band positions with medium-weak intensities were obtained for this region and were visualized at 1127 cm^{-1}, 1086 cm^{-1}, and 1011 cm^{-1} for theoretical spectrum. Bands comprised between 1044 and 975 cm^{-1} region were usually strongest in the Raman spectrum and present a weak/medium intensity in the IR spectrum for mono-substituted aromatic ring. As it was expected, in the experimental infrared, most signals with medium/weak intensity at 1113 cm^{-1} (medium), 1076 cm^{-1} (medium), 1028 cm^{-1} (weak), and 996 cm^{-1} (weak) were observed.

In the experimental Raman spectrum, the bands assigned to the CH *oop* and ring torsion (tri-subst. R_3-C_6H_3), both coupled to aromatic-Si bending, are related with two vibrations, and these signals appear at 943 (weak), 873 cm^{-1} (weak), respectively. DFT calculations predict the bands centered at 929 cm^{-1} and 884 cm^{-1}, both values with weak intensities. These same signals were observed in the experimental infrared spectra at 921 cm^{-1} and 825 cm^{-1} with medium-weak and weak intensities, respectively.

For the case of the secondary amide, the *oop* NH wagging band is located in the 750–700 cm^{-1} region for associated open-chain amide.[42] Additionally, using DFT methods, CH *oop* bending mono-subst. R-C_6H_5 coupled with NH *oop* wagging appears with weak intensities at 742 cm^{-1} and 710 cm^{-1}. These results are: 741 cm^{-1} (mw) and 700 cm^{-1} (m) for the experimental infrared data and 771 cm^{-1} (w) for experimental Raman results.

Finally, below 700 cm^{-1}, there are some peaks associated to ring deformation modes of mono- and tri-substituted aromatic rings. Thus, Theoretical spectra show bands at 653 cm^{-1} (weak). Additionally, experimental Raman and infrared spectrum shows this vibration mode at 672 cm^{-1} (medium-weak) and at 601 cm^{-1} (weak), respectively.

Theoretically predicted wavenumbers using B3LYP/6-31G* theory are similar to the experimental data obtained (Fig. 5). Thus, the experimental vibrations showed by the aromatic ring (CH and C=C stretching), C=O, CH_3, OH and CH (*oop* and *ip*) bending present a similitude with the results obtained by this method. However, theoretical DFT studies show pronounced bands near to 3000 cm^{-1}, corresponding to the aromatic CH stretching. This same signal appears with weak intensity using experimental techniques, difference that is related to the noise produced by oligomer fluorescence. This behavior is related to resonance effect, attributed to symmetric *ip* vibration of the conjugated ring systems. The electronic state is one of the parameters that can affect the spectral profile (higher electronic resonance at higher planarity). Therefore, the polymer backbone and its side chain or intermolecular interactions between them could affect the vibrational modes (displacement and their intensity) of the whole polymer.

It is noteworthy that the difference in the frequencies of the calculated and experimental spectra also could be explained in the methodology utilized for study the vibrational modes; the calculations are performed for isolated molecules (in the gas phase), and the experimental spectra are measured in solid state.

Conclusion

Experimental and theoretical spectra of monomer (**L-VAL**) and its respective oligomer polyamide-imide (**PALV**) were studied. The predicted wavenumbers were calculated using B3LYP/6-31G* as base model. Thus, the vibrational modes were determined and compared with experimental results. The respective spectral positions of certain vibrations were predicted by DFT calculations, allowing a proper assignment of the signals in the expected range for experimental analysis. However, the molecular optimization geometry of the monomer/oligomer was studied in vacuum via DFT method, producing differences in the displacement of certain signals in the spectra. This effect makes it impossible to detect intramolecular interactions and very weak intermolecular interactions; only spectral correlation can be observed. In addition, the experimental values of the vibrational natural frequencies show a certain similitude with the results obtained through the DFT theoretical method. This behavior is observable in the aromatic ring vibrations such as CH stretching and CH bending.

Oligomer presents the amide I and III bands with their respective skeletal vibration, results that suggest a randomly disordered conformation in the solid state. Additionally, the monomer **L-VAL** shows higher intensity of certain vibrations of the aromatic rings that are related to a flat orientation breakage of the phenyl groups bonded to silicon central atom. Thus, the alignment of the oligomeric chain is mainly achieved by the distortion of coplanar phenyl groups bonded to silicon

atoms. Likewise, in this process, the rearrangement of the amide dipoles into the oligomeric structure is an important process that is mainly associated to the backbone torsion through CN linkages.

Acknowledgments

C. M. González-Henríquez acknowledges the financial support provided by FONDECYT (grant 11121281) and to the Attraction and Insertion of Advanced Human Capital Program (PAI) by CONICYT (grant 7912010031). Theoretical calculations were realized by Dr. Jose Vicente Correa, Laboratory of Theoretical and Computational Chemistry, Pontificia Universidad Católica de Chile. C. A. Terraza acknowledges the financial support provided by FONDECYT (grant 1150157). Raman spectroscopy was supported by FONDEF project N° D97F1001 (PUC). M. A. Sarabia acknowledges the financial support given by CONICYT through the Doctoral Scholarship Grant. Finally, A. E. Aliaga acknowledges the financial support given by the CONICYT/FONDECYT Postdoctoral Project 3140492. Finally, this work/study was funded by VRAC Grant Number L216-04 of Universidad Tecnológica Metropolitana.

References

[1] Giussani, E.; Fazzi, D.; Brambilla, L.; Caironi, M.; Castiglioni, C. Molecular level investigation of the film structure of a high electron mobility copolymer via vibrational spectroscopy. *Macromolecules* **2013**, *46*(7), 2658–2670. doi:10.1021/ma302664s.

[2] Lahr, R. H.; Vikesland, P. J. Surface-enhanced raman spectroscopy (SERS) cellular imaging of intracellulary biosynthesized gold nanoparticles. *ACS Sustainable Chemistry and Engineering* **2014**, *2*(7), 1599–1608. doi:10.1021/sc500105n.

[3] Centeno, S. A. Identification of artistic materials in paintings and drawings by Raman spectroscopy: Some challenges and future outlook. *Journal of Raman Spectroscopy* **2016**, *47*(1), 9–15. doi:10.1002/jrs.4767.

[4] Edwards, H. G. *Raman Spectroscopic Analysis of Art and Archaeological Materials. In Encyclopedia of Analytical Chemistry*; John Wiley & Sons, Ltd: Chichester, UK, n.d., 1–19. doi:10.1002/9780470027318.a9504.

[5] Doty, K. C.; Muro, C. K.; Bueno, J.; Halámková, L.; Lednev, I. K. What can Raman spectroscopy do for criminalistics? *Journal of Raman Spectroscopy* **2016**, *47*(1), 39–50. doi:10.1002/jrs.4826.

[6] Wang, W.; Zhao, J.; Short, M.; Zeng, H. Real-time in vivo cancer diagnosis using raman spectroscopy. *Journal of Biophotonics* **2015**, *8*(7), 527–545. doi:10.1002/jbio.201400026.

[7] Sebastian, S. S.H. R.; Al-Tamimi, A. M.S.; El-Brollosy, N. R.; El-Emam, A. A.; Yohannan Panicker, C.; Van Alsenoy, C. Vibrational spectroscopic (FT-IR and FT-Raman) studies, HOMO-LUMO, NBO analysis and MEP of 6-methyl-1-({[(2E)-2-methyl-3-phenyl-prop-2-en-1-yl] oxy} methyl)-1,2,3,4-tetra-hydroquinazoline-2,4-dione, a potential chemotherapeutic agent, using density functio. *Spectrochimica Acta - Part A: Molecular and Biomolecular Spectroscopy* Elsevier B.V.: **2015**, *134*, 316–325. doi:10.1016/j.saa.2014.06.039.

[8] Schmidt, M. A.; Kiefer, J. Polarization-resolved high-resolution Raman spectroscopy with a light-emitting diode. *Journal of Raman Spectroscopy* **2013**, *44*(11), 1625–1627. doi:10.1002/jrs.4385.

[9] Huang, C.; Kim, M.; Wong, B. M.; Safron, N. S.; Arnold, M. S.; Gopalan, P. Raman enhancement of a dipolar molecule on graphene. *Journal of Physical Chemistry C* **2014**, *118*(4), 2077–2084. doi:10.1021/jp410749a.

[10] Ngo, Y. H.; Li, D.; Simon, G. P.; Garnier, G. Gold nanoparticle-paper as a three-dimensional surface enhanced Raman scattering substrate. *Langmuir: The ACS Journal of Surfaces and Colloids* **2012**, *28*, 8782–8790. doi:10.1021/la3012734.

[11] González-Henríquez, C. M.; Terraza, C. A.; Sarabia, M. Theoretical and experimental vibrational spectroscopic investigation of two R1R2-diphenylsilyl-containing monomers and their optically active derivative polymer. *Journal of Physical Chemistry A* **2014**, *118*(7), 1175–1184. doi:10.1021/jp409178j.

[12] Arivazhagan, M.; Manivel, S.; Jeyavijayan, S.; Meenakshi, R. Vibrational spectroscopic (FTIR and FT-Raman), first-order hyperpolarizablity, HOMO, LUMO, NBO, Mulliken charge analyses of 2-ethylimidazole based on Hartree-Fock and DFT calculations. *Spectrochimica Acta – Part A: Molecular and Biomolecular Spectroscopy* Elsevier B.V.: **2015**, *134*, 493–501. doi:10.1016/j.saa.2014.06.108.

[13] Partal Ureña, F.; Avilés Moreno, J. R.; López González, J.J. Conformational flexibility in terpenes: vibrational circular dichroism (VCD), infrared and Raman study of S -(–)-perillaldehyde. *The Journal of Physical Chemistry A* **2008**, *112*(34), 7887–7893. doi:10.1021/jp801099e.

[14] Jacob, C. R.; Luber, S.; Reiher, M. Analysis of secondary structure effects on the IR and Raman spectra of polypeptides in terms of localized vibrations. *The Journal of Physical Chemistry B* **2009**, *113*(18), 6558–6573. doi:10.1021/jp900354g.

[15] Lin, G.-Q.; Zhang, J.-G.; Cheng, J.-F. Overview of chirality and chiral drugs. In *Chiral Drugs*, 1st ed; Lin, G.-Q., You, Q.-D., Cheng, J.-F., Eds.; John Wiley & Sons, Inc.: Hoboken, NJ, USA, 2011, 3–28. doi:10.1002/9781118075647.

[16] Ulrich, E. M.; Falconer, R. L. Chiral chlordane components in environmental matrices. *ACS Symposium Series* **2011**, *1085*(July), 11–43. doi:10.1021/bk-2011-1085.ch002.

[17] González Henríquez, C. M.; Tagle, L. H.; Terraza, C. A.; Barriga González, A.; Volkmann, U. G.; Cabrera, A. L.; et al. Structural symmetry breaking of silicon-containing poly(amide-imide) oligomers and its relation to electrical conductivity and Raman-active vibrations. *Polymer International* **2012**, *61*(2), 197–204. doi:10.1002/pi.3169.

[18] Kataoka, S.; Atagi, K. Preventing IR interference between infrared waves emitted by high-frequency fluorescent lighting systems and infrared remote controls. *IEEE Transactions on Industry Applications* **1997**, *33*(1), 239–245. doi:10.1109/28.567122.

[19] Martin, E. J. J.; Bé, N.; Provencher, F.; Cô, M.; Silva, C.; Doorn, S. K.; et al. Resonance Raman spectroscopy and imaging of push–pull conjugated polymer–fullerene blends. *Journal of Materials Chemistry C* **2015**, *3*(0), 6058–6066. doi:10.1039/C5TC00847F.

[20] Geitner, R.; Kö, J.; Siegmann, M.; Bocklitz, T. W.; Hager, M. D.; Schubert, U. S.; et al. Two-dimensional Raman correlation spectroscopy reveals molecular structural changes during temperature-induced self-healing in polymers based on the Diels–Alder reaction. *Physical Chemistry Chemical Physics* **2015**, *17*(17), 22587–22595. doi:10.1039/C5CP02151K.

[21] Tagle, L. H.; Terraza, C. A.; Tundidor-Camba, A.; Ortiz, P. A. Silicon-containing oligomeric poly(imido-amides) with amino moieties. Synthesis, characterization and thermal studies. *RSC Advances* **2014**, *4*(57), 30197–30210. doi:10.1039/C4RA04291C.

[22] Pratt, J. R.; Thames, S. F. Organosilicon compounds. XVIII. Silicon-containing dianhydrides. *The Journal of Organic Chemistry* **1973**, *38*(25), 4271–4274. doi:10.1021/jo00964a013.

[23] González Henríquez, C. M.; Terraza, C. A.; Tagle, L. H.; Barriga González, A.; Volkmann, U. G.; Cabrera, A. L.; et al. Inclusion effect of gold and copper particles in a poly(amide) matrix that contains a thiophene moiety and Si or Ge atoms in the main chain. *Journal of Materials Chemistry* **2012**, *22*, 6782–6791. doi:10.1039/c2jm16083h.

[24] Yamazaki, N.; Matsumoto, M.; Higashi, F. Studies on reactions of the N-phosphonium salts of pyridines. XIV. Wholly aromatic polyamides by the direct polycondensation reaction by using phosphites in the presence of metal salts. *Journal of Polymer Science: Polymer Chemistry Edition* **1975**, *13*(6), 1373–1380. doi:10.1002/pol.1975.170130609.

[25] Terraza, C. A.; Tagle, L. H.; Tundidor-Camba, A.; González-Henríquez, C. M.; Coll, D.; Sarabia, M. M. Silarylene-containing oligo(ether-amide)s based on bis(4-(4-amino phenoxy)phenyl) dimethylsilane. Effect of the dicarboxylic acid structure on some properties. *RSC Advances* **2015**, *5*(36), 28515–28526. doi:10.1039/C5RA03529E.

[26] Frisch, M. J.; Trucks, G. W.; Schlegel, H. B.; Scuseria, G. E.; Robb, M. A.; Cheeseman, J. R.; Montgomery, Jr., J. A.; Vreven, T.; Kudin, K. N.; Burant, J. C.; Millam, J. M.; Iyengar, S. S.; Tomasi, J.; Barone,

V.; Mennucci, B.; Cossi, M.; Scalmani, G.; Rega, N.; Petersson, G. A.; Nakatsuji, H.; Hada, M.; Ehara, M.; Toyota, K.; Fukuda, R.; Hasegawa, J.; Ishida, M.; Nakajima, T.; Honda, Y.; Kitao, O.; Nakai, H.; Klene, M.; Li, X.; Knox, J. E.; Hratchian, H. P.; Cross, J. B.; Bakken, V.; Adamo, C.; Jaramillo, J.; Gomperts, R.; Stratmann, R. E.; Yazyev, O.; Austin, A. J.; Cammi, R.; Pomelli, C.; Ochterski, J. W.; Ayala, P. Y.; Morokuma, K.; Voth, G. A.; Salvador, P.; Dannenberg, J. J.; Zakrzewski, V. G.; Dapprich, S.; Daniels, A. D.; Strain, M. C.; Farkas, O.; Malick, D. K.; Rabuck, A. D.; Raghavachari, K.; Foresman, J. B.; Ortiz, J. V.; Cui, Q.; Baboul, A. G.; Clifford, S.; Cioslowski, J.; Stefanov, B. B.; Liu, G.; Liashenko, A.; Piskorz, P.; Komaromi, I.; Martin, R. L.; Fox, D. J.; Keith, T.; Al-Laham, M. A.; Peng, C. Y.; Nanayakkara, A.; Challacombe, M.; Gill, P. M. W.; Johnson, B.; Chen, W.; Wong, M. W.; Gonzalez, C.; and Pople, J. A. Gaussian, Inc., Wallingford, CT, 2004.

[27] Francl, M. M. Self-consistent molecular orbital methods. XXIII. A polarization-type basis set for second-row elements. *The Journal of Chemical Physics* **1982**, *77*(7), 3654. doi:10.1063/1.444267.

[28] Wong, M. W. Vibrational frequency prediction using density functional theory. *Chemical Physics Letters* **1996**, *256*(4–5), 391–399. doi:10.1016/0009-2614(96)00483-6.

[29] Rauhut, G.; Pulay, P. Identification of isomers from calculated vibrational-spectra – a density-functional study of tetrachlorinated dibenzodioxins. *Journal of the American Chemical Society* **1995**, *117*(14), 4167–4172. doi:10.1021/ja00119a034.

[30] Hutter, J.; Lüthi, H. P.; Diederich, F. Structures and vibrational frequencies of the carbon molecules C2-C18 calculated by density functional theory. *Journal of the American Chemical Society* **1994**, *116*(2), 750–756. doi:10.1021/ja00081a041.

[31] Bozovic, I. B.; Vujicic, M.; Herbut, F. Irreducible representations of the symmetry groups of polymer molecules. I. *Journal of Physics A: Mathematical and General* **1978**, *11*(11), 2133–2147. doi:10.1088/0305-4470/11/11/003.

[32] Socrates, G. The carbonyl group: C=O. In *Infrared and Raman Characteristic Group Frequencies. Tables and Charts*, 3rd ed.; Wiley & Sons Ltd.: New York, 2004, 115–154.

[33] Roeges, N. P. G. Normal vibrations and absorption regions of ring structures. In *A Guide to the Complete Interpretation of Infrared Spectra of Organic Structures*; John Wiley & Sons, Ltd: New York, 1994, 301–334.

[34] Mendelovici, E.; Frost, R. L.; Kloprogge, J. T. Modification of Chrysotile Surface by Organosilanes: An IR–photoacoustic spectroscopy study. *Journal of Colloid and Interface Science* **2001**, *238*(2), 273–278. doi:10.1006/jcis.2001.7524.

[35] Lin-Vien, D.; Colthup, N. B.; Fateley, W. G.; Grasselli, J. G. Alkanes. In *The Handbook of Infrared and Raman Characteristic Frequencies of Organic Molecules;* 1st ed.; Elsevier, 1991, 9–28. doi:10.1016/B978-0-08-057116-4.50008-0.

[36] Sánchez-Cortés, S.; García-Ramos, J. Adsorption and chemical modification of phenols on a silver surface. *Journal of Colloid and Interface Science* **2000**, *231*(1), 98–106. doi:10.1006/jcis.2000.7101.

[37] Durig, J. R.; Larsen, R. A.; Kelley, R.; Sun, F.-Y.; Li, Y.-S. Raman and infrared spectra, conformational stability and vibrational assignment for 1,1,1-trifluoro-2-methoxypropane. *Journal of Raman Spectroscopy* **1990**, *21*(2), 109–122. doi:10.1002/jrs.1250210208.

[38] Yang, X.; Orlova, G.; Zhou, X. J.; Leung, K. T. A DFT study on the radical, monomer and dimer of α-keto pyruvic acid: equilibrium structures and vibrational analysis of stable conformers. *Chemical Physics Letters* **2003**, *380*(1–2), 34–41. doi:10.1016/j.cplett.2003.09.001.

[39] McColl, I. H.; Blanch, E. W.; Hecht, L.; Barron, L. D. A study of α-helix hydration in polypeptides, proteins, and viruses using vibrational Raman optical activity. *Journal of the American Chemical Society* **2004**, *126*(26), 8181–8188. doi:10.1021/ja048991u.

[40] Myshakina, N. S.; Ahmed, Z.; Asher, S. A. Dependence of amide vibrations on hydrogen bonding. *Journal of Physical Chemistry B* **2008**, *112*(38), 11873–11877. doi:10.1021/jp8057355.

[41] Yamamoto, S.; Kaminský, J.; Bouř, P. Structure and vibrational motion of insulin from Raman optical activity spectra. *Analytical Chemistry* **2012**, *84*(5), 2440–2451. doi:10.1021/ac2032436.

[42] Dollish, F. R.; Fateley, W. G.; Bentley, F. F. *Characteristics Raman Frequencies of Organic Compounds*; Wiley-VCH: New York, 1974.